


Enhanced Josephson coupling in hybrid nanojunctionsDomenico Montemurro ^{1,2,*}, Dmitry S. Golubev,³ Sergey Kubatkin,¹ Francesco Tafuri,²
Thilo Bauch,¹ and Floriana Lombardi¹¹*Quantum Device Physics Laboratory, Department of Microtechnology and Nanoscience,
Chalmers University of Technology, SE-41296 Göteborg, Sweden*²*Dipartimento di Fisica “Ettore Pancini,” Università di Napoli “Federico II,” Monte S. Angelo, I-80126 Napoli, Italy*³*Low Temperature Laboratory (OVLL), Aalto University School of Science, P.O. Box 13500, FI-00076 Aalto, Finland*

(Received 19 July 2022; revised 27 December 2022; accepted 7 March 2023; published 23 March 2023)

We have fabricated NbN/Au nanogaps and bridged them with an Al superconductor using Ti as an interlayer. The nanodevices show a critical current density at 300 mK as high as 3×10^6 A/cm², which is 30% higher than that of Al nanowires with the same lateral dimensions as the NbN-based devices. The response of the critical current as a function of the external magnetic field clearly showed a Fraunhofer-like behavior, indicating a Josephson coupling between the NbN electrodes through the Al barrier. The superconducting transport evolves into different transport regimes as a function of the temperature. These findings demonstrate the importance of using superconducting barriers in hybrid nanodevices to achieve very high Josephson current in nanodevices of great relevance in superconducting circuits requiring high integration density.

DOI: [10.1103/PhysRevB.107.094517](https://doi.org/10.1103/PhysRevB.107.094517)**I. INTRODUCTION**

Advances in material science and nanofabrication have favored the development of a new class of hybrid Josephson junctions (JJs) in which a much wider variety of barriers than in the past is integrated with superconducting electrodes [1–9]. Here “hybrid” stands for a barrier which, different from a simple insulator or a normal metallic layer, can add novel functionalities to the Josephson coupling, transferring the specific—possibly unconventional—features of the barrier to the coherent flow of the carriers such as topological states, ferroelectricity, magnetoelectricity, noncollinear magnetism, and emergent properties from twisted heterostructures. Barriers leading to hybrid JJs are, for instance, ferromagnets [10–14], semiconductors [15–26], topological insulators [27–31], graphene [32,33], nanotubes [34,35], etc., and are really driving exciting research in different directions. Their major complexity requires additional efforts to engineer the final layout of the junctions, and the literature is very rich with experimental and theoretical studies on very advanced and complex structures. Interfaces are the key element to determine the overall properties of the junctions. They are the primary sites where electrodes and barriers match with the opportune boundary conditions. The junction properties will depend not only on their inner nature but

also on the properties of the barrier, on the superconducting electrodes and on the conditions under which they are built. They will operate as filters for the competing processes occurring in the junctions, with the possible unavoidable result of introducing artifacts and, in some cases, with extreme consequence of hiding specific effects associated with the special barrier/superconductor ensemble. These notions are well documented for all classical JJs, including high critical temperature superconductor JJs [36]. Perfect interfaces have never been as necessary as they are now in order to have access to several key phenomena [17,30,37,38]. The primary criteria to measure the efficiency of a barrier is its transparency, which is the ultimate aim of the present study. Highly transparent barriers also imply a much stronger proximity effect and tend to be a solution for another wider class of applications where higher values of critical currents are required, such as in digital circuits [17,39–41]. Here we present devices based on NbN nanogaps which are bridged with an Al superconductor that in this case works as a barrier. We use a combination of Au and Ti layers in between the electrodes and the barrier to improve the interface resistance. The concept of using an intermediate layer to match very different materials has been exploited in different contexts and for different types of Josephson junctions, mostly in multilayer and coplanar structures. Protecting layers have also been used for high critical temperature superconductor (HTS) thin films due to the ease of the degradation of properties at the surfaces [36]. Following this approach, we have been able to achieve a Josephson critical current exceeding the critical current values of Al nanowires. Another advantage to making devices based on nanogaps is represented by the possibility to build junctions in suspended architecture. This means that the barrier material is surrounded by vacuum, suggesting that there is no coupling with the substrate. Because of that no

*domenico.montemurro@unina.it

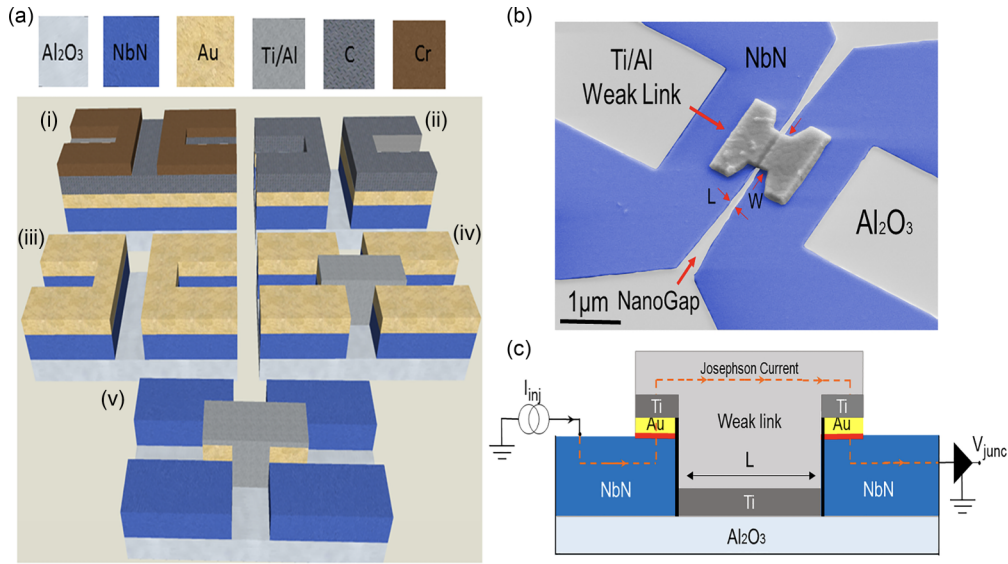


FIG. 1. (a) Fabrication flow. (i) A 40 nm thick NbN film is epitaxially grown and capped by a uniform Au layer 10 nm thick. All devices have a gap length L of the order of 100 nm and a width W of 1 μm , while the thickness t of the deposited (Au or Al) barrier is 145 nm (see Table I). By pulsed laser deposition an 80 nm thick C hard mask is deposited. The first EBL step transfers the design of the device through a liftoff of a 12 nm Cr mask. (ii) IBE step defines the geometry of the device. (iii) The C layer is removed by a gentle oxygen plasma etching. (iv) Resists are exposed; prior to the Ti/Al evaporation a gentle oxygen plasma etching is accomplished. (v) The Second IBE step removes 10 nm of Au; the Au thin layer is only kept under the Ti/Al weak link. (b) False 30° tilted scanning electron microscope micrograph of a typical NbN/Au-Ti/Al-NbN/Au junction. (c) Cross section of the junction; the I_C path (orange dashed line) is displayed. The horizontal red and vertical black lines represent two tunable barriers that allow us to fix the current's path in the built junctions. In our case, with test devices we have proven that the vertical black lines in the NbN nanogap sidewall have the lowest transparency.

accumulation layer pops up; thus, in the case of a barrier made by topological insulators (Weyl and Dirac semimetals such as BiSe and HgTe) its surface states, which are responsible for the transport properties, are not affected by any charge due to the interaction with the substrate [30,42].

In this work the notion of interposing layers is specifically studied for nanojunction layouts based on nanogaps [43–48]. The overall studied structures are NbN/Au-Ti/Al/Ti/Au/NbN, as shown in Fig. 1(a). By the proximity effect [49], Cooper pairs diffuse from the superconducting

banks (S) with a higher superconducting gap, which in our case is NbN with a critical temperature $T_C^{\text{NbN}} \sim 16$ K, to the superconducting Al (S') barrier (our evaporated Al has $T_C^{\text{Al}} \sim 1.05$ K). The supercurrent [dashed orange lines in Fig. 1(c)] passes across the most transparent interfaces of the junction [red line in Fig. 1(c)], those with the Au-Ti interlayer. We rule out that there are any supercurrent flows in the region where the NbN is in direct contact with the Al barrier since electrical measurements performed on test devices showed a highly resistive NbN/Al interface that completely hampered

TABLE I. The devices are gathered in three groups (A, B, and C); NbN nanogaps belonging to groups A and B are covered by 10 nm thick Au, while the Al test nanowires are included in group C. Chips A, B, and C were fabricated following the procedure reported in Sec. II. Junction parameters L , W , R_N^{junc} , $I_C^{300\text{mK}}$, $J_C^{300\text{mK}}$, and $I_C R_N$ represent the space between two NbN superconducting banks, the width of the (Al or Au) barrier, the normal resistance, the critical current and critical current density at $T = 300$ mK, and the product of the critical current and normal resistance, respectively. Next, R_B , R_C , and T_C represent the barrier resistance, the interface resistance, and the critical temperature of the junction, respectively. The characteristic parameters for Al test nanowires fabricated on the same chip as the junctions are also included. For all the reported junctions the thicknesses of NbN (t^{NbN}), Al (t^{Al}), and Ti (t^{Ti}) layers are, respectively, 40, 145, and 12 nm. The contact area between the NbN banks and the Au or Al barriers equals $S_C = 2.46 \mu\text{m}^2$. The critical temperatures of NbN and Al are 16 and 1.05 K, respectively. The values of L and W were determined from the scanning electron microscope image. The Al test nanowires were fabricated on the same sapphire chip as the NbN/Al junctions, and they have the same thickness, $t = 145$ nm, as the Al bridges in the NbN nanogaps.

Chip	Device	L (nm)	W (μm)	R_N^{junc} (m Ω)	$I_C^{300\text{mK}}$ (mA)	$J_C^{300\text{mK}}$ (MA/cm 2)	$I_C R_N$ (μV)	R_B (m Ω)	R_C (m Ω)	T_C
A	NbN/Al-E2	100	1	81	4.70	3.24	381	31	19	5.0
A	NbN/Al-C5	90	1	105	4.56	3.14	479	44	17	5.0
A	NbN/Al-C4	80	1	100	5.30	3.65	530	42.5	15	5.0
A	NbN/Al-B2	360	1	400	1.41	0.97	564	165	70	1.9
A	NbN/Al-B2	360	1	400	0.104 ($T = 1.15$ K)	0.07 ($T = 1.15$ K)	41 ($T = 1.15$ K)	165	70	1.9
B	NbN/Au-B2	230	2×0.5	400	0.0026	0.0018	1	180	40	0.9
C	Al-NW	5000	0.2	2150 ($T = 2$ K)	0.7	2.4	1500			1.05

a current from passing through it. When the NbN is in direct contact with the Al barrier, by the proximity effect, their density of states at the interface affects each other [1]. The former mechanism shows a strong dependence on the interface quality between the coupled materials that could influence the transport properties of the junction [50]. A Cooper pair penetrates the normal material (N) coherently propagating as a time-reversed electron-hole pair in N if the length L of N is shorter than its normal coherent length ξ_N [51]. We find that the transparency of the built junctions depends on the two main parameters: the annealing temperature and the thickness of the used Au capping layer of the NbN banks. Fixing the Au annealing temperature at 400 °C for the NbN banks, which are covered by a 5 nm thick Au layer, leads the junctions to show critical current density (J_C) of the order of tens of KA/cm² with an $I_C R_N$ product (where I_C is the critical current and R_N is the normal resistance) of a few hundred μ V (see chip C in Table I). By increasing the thickness of Au up to 10 nm we were able to build junctions with higher transparency: J_C and the $I_C R_N$ product are three orders of magnitude and a factor of 2 higher than the values measured in devices covered by a thinner Au layer, respectively. Table I summarizes the main parameters collected on annealed devices at 400 °C with an Au capping layer 10 nm thick.

For temperatures $T_C^{\text{Al}} < T < T_C^{\text{NbN}}$, such a NbN/Al system is expected to behave as a superconductor-normal-superconductor (S-N-S) junction, and it is well established that the supercurrent in such a system is predominantly carried through Andreev levels [51]. Below T_C^{Al} , we have modeled our device as two S-I-S' junctions in series, where I indicates the interface between the NbN and the proximized Au-Ti-Al layer. We have also made a comparative analysis of NbN nanojunctions bridged by Al barriers with those bridged by an Au weak link. We find that NbN/Al Josephson junctions exhibit long-range proximity-induced superconductivity in Al barriers. These results are supported by our theoretical modeling of the nanojunctions (see Appendix B). Apart from the technical aspects sketched above and extensively discussed in the sections below, this experiment gives an example of how to induce a giant proximity effect by increasing the critical current density and the critical temperature of an Al nanostructure inserted in a Josephson structure. Al technology is the main one for all current superconducting technologies, and this experiment suggests a way not only to enhance the performances of the device but also to enlarge the space of the parameters of operation for all coplanar hybrid junctions. These are widely employed in a variety of cutting-edge experiments aimed at investigating the topological phases of matter and their unconventional excitations like Majorana fermions and would benefit from operating in a wider range of conditions to remove possible ambiguities. Also, simple Al nanowires widely studied in the literature [52–54] would benefit from operating at higher temperatures and values of the current.

II. FABRICATION

We fabricated NbN nanogaps with lengths ranging from 80 to 230 nm. NbN thin films were epitaxially grown on a (110)-oriented sapphire substrate in ultrahigh vacuum by DC

magnetron sputtering from a high-quality Nb target. Prior to the NbN deposition the substrate was annealed at 780 °C for 30 min, and 2 nm of Nb were deposited. Then the substrate was cooled down to room temperature, and an additional 38 nm of NbN were sputtered. A flux of 6.5 sccm of N_2 at a pressure of 6.7 μ bar was allowed to achieve $T_C \sim 16$ K. To prevent the oxidation of the NbN surface, *in situ*, we deposited a thin layer of Au acting as a NbN cap layer. The deposition conditions of Au have proved to be crucial for the transparency of the interfaces. The Au layer was sputtered at 400 °C on the NbN film [55,56]. Previous works showed that at this temperature the transparency between the two layers (NbN and Au) is increased compared to that achieved by depositing Au at room temperature.

The nanogaps (NGs) in the NbN/Au bilayer [see the false scanning electron microscope image in Fig. 1(b)] are fabricated by using a carbon mask in combination with an electron-beam lithography (EBL) step and a gentle Ar ion-beam etching (IBE) [57]. The geometrical parameters of the NGs are summarized in Table I. The NGs are then bridged by a (12 nm) Ti/(145 nm) Al bilayer, whose geometry is defined by a second EBL followed by a liftoff step. The Ti interlayer improves the adhesion between the Au and Al layers and reduces the mismatch of the Fermi energies [58]. Figure 1(a) shows the sketch of the entire fabrication process. To highlight the unique properties of the superconducting proximity effect induced in a superconducting barrier, we also fabricated NGs bridged with Au for comparison.

III. EXPERIMENTAL RESULTS

A. Normal transport properties

The transport properties of the junctions were studied using four probe electrode geometries in a ³He refrigerator with a base temperature of 300 mK. The cryostat was equipped with a superconducting solenoid providing magnetic field up to 70 mT. The thickness of the NbN banks t^{NbN} , the NG length L , the thickness of the Al barrier t^{Al} , and the width of the Josephson junctions W are given in the caption of Table I. The surface area of the contact barrier $S_C = 2.46 \mu\text{m}^2$ was estimated from the scanning electron microscope image. Due to their exposure to air prior to deposition of the bridges, the sidewalls of the NbN NGs form low-transparency interfaces with the metals (Ti/Al or Ti/Au). We have tested this assumption by making NbN-based NGs without the Au capping layer, and none of those devices showed measurable current at 300 mK. Thus, we conclude that the current path follows the direction sketched by the orange dashed line in Fig. 1(c).

1. NbN/Al and Al nanowire

Here we compare the superconducting properties of the NbN/Al junctions with those employing Au as the barrier in the NbN nanogaps (NbN/Au). The Josephson current in these two configurations is also compared with the critical current of a pure Al nanowire (Al-NW; see Table I). This comparison provides clear evidence of enhanced superconductivity in the barrier made of the superconducting material, which will be discussed below. Figure 2 shows the current density J_C as a function of the bias voltage for the NbN/Al-E2

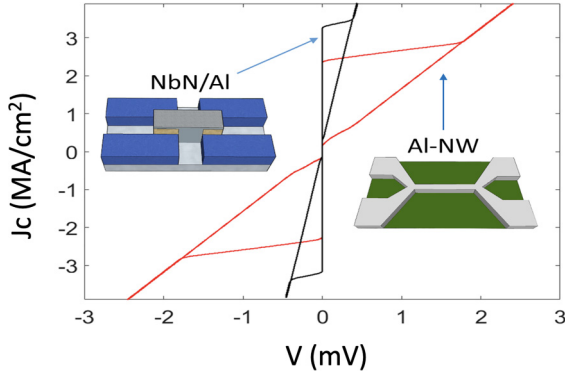


FIG. 2. J_C - V curves of the 200 nm wide and 145 nm thick Al nanowire (red line) and NbN/AI-E2 Josephson junction (black line). Both devices are grown on the same sapphire substrate. The curves were recorded at $T = 300$ mK. The geometry of the nanowire has been adjusted to avoid the current crowding effects [59].

junction (black curve) and for a pure Al-NW (red curve). Al-NWs were fabricated on the same chip as the NbN/AI junctions. At $T = 300$ mK we obtain the critical current density $J_C^{\text{NbN/AI}} = 3.2$ MA/cm² for the junction NbN/AI-E2, while $J_C^{\text{Al}} = 2.4$ MA/cm² for the Al nanowire. We estimate that $J_C^{\text{NbN/AI}}$ is $\sim 33\%$ times higher than $J_C^{\text{Al-NW}}$. This confirms that the proximity effect enhances the superconducting properties of the Al barrier bridging the NGs between the NbN banks.

To test our assumption about proximity-enhanced superconductivity in Al barriers further, we fabricated a batch of junctions with gold bridges over the NbN NGs. In Fig. 3, we compare the transport properties of the two junctions NbN/Au-B2 and NbN/Al-B2, which have the same layout and similar interface transparency between the electrodes and the barrier material. In Fig. 3 we show the critical currents of the two junctions versus temperature $I_C(T)$. Both junctions have the same R_N^{junc} at room temperature but have different lengths L of the NG channel. The corresponding

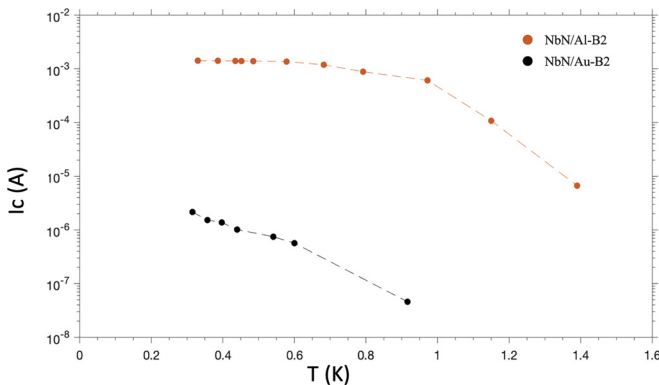


FIG. 3. I_C - T curves for junctions based on NbN nanogaps employing Al (NbN/Al-B2; red points) and Au (NbN/Au-B2; black points) as a barrier. NbN/Au-B2 has a superconducting quantum interference device design, and its width, due to the sum of the widths of two single junctions, is equal to that of the NbN/Al-B2 junction. NbN/Al-B2 has $T_C \sim 1.9$ K, while NbN/Au-B2 has $T_C \sim 0.9$ K. Other parameters are reported in Table I.

values are given in Table I: $L^{\text{NbN/Al}} = 360$ nm and $L^{\text{NbN/Au}} = 230$ nm. Taking the values of resistivity for gold, $\rho_{\text{Au}} = 2.4 \times 10^{-8}$ Ω m, and for aluminum, $\rho_{\text{Al}} = 3 \times 10^{-8}$ Ω m, we estimate the channel resistance of the NbN/Au-B2 junction as $R_C \sim 40$ m Ω , and for junction NbN/Al-B2 we obtain $R_C \sim 70$ m Ω . Since the total resistance of the junctions is expressed as $R_N^{\text{junc}} = 2R_B + R_C$ [60], where R_B is the interface resistance, we obtain similar values of R_B for both junctions, and therefore, we can expect the two junctions to have similar interface transparencies (see Table I). Even though the interface resistances R_B are similar for both junctions, the NbN/Al-B2 junction is longer than the NbN/Au-B2 one. Despite that, the junction with the aluminum bridge has a significantly higher critical current (see Fig. 3). Indeed, junction NbN/Au-B2 has $I_C^{\text{NbN/Au}} \sim 2.6$ μ A and $T_C \sim 0.9$ K, while for junction NbN/Al-B2 $I_C^{\text{NbN/Al}}(1.4 \text{ K}) \sim 6.5$ μ A and $T_C \sim 1.9$ K. $I_C^{\text{NbN/Al}}(1.4 \text{ K})$ is almost 3 times higher than $I_C^{\text{NbN/Au}}$ at 300 mK (see Fig. 3). These results are in line with previous theoretical and experimental works, which also showed that the intrinsic superconducting correlations in a film have a strong influence on the proximity-induced superconductivity [2,61,62]. Devices NbN/Al-B2 and NbN/Au-B2 were also studied in the presence of magnetic field, and those results are presented in Appendix A. The junctions were further characterized by measuring the current-voltage characteristics (IVCs) at various temperatures and magnetic fields. The magnetic field was always applied orthogonal to the direction of the critical current that passes through the barrier. In Fig. 4 we show the IVCs for junction NbN/Al-E2 at zero magnetic field. The current voltage curves turn out to be highly hysteretic. The hysteretic behavior of the IVCs could be ascribed to self-heating as a cause of the substantially reduced retrapping I_r below the value of the up-sweep I_s . This could generate Joule heating that is not entirely dissipated by either the NbN superconducting banks or the substrate. Former phenomena entail that current higher than the supercurrent leads to an increase in the effective electrons's temperature, thus reducing the amplitude of the retrapping current during the bias down sweep [63].

2. Critical current: Temperature dependence

In this section, we discuss the temperature dependence of the critical current for junction NbN/Al-E2. We model the system as an SIS/IS structure, where S stands for superconducting leads made of NbN, S' denotes the Al bridge, and I denotes the barrier between NbN and Al, i.e., the Ti/Au bilayer. A full theory for our device would require the numerical solution of Usadel's equation [64]. Here we will use a simplified model, which is sufficient to describe the transport properties of the junctions at temperatures below the critical temperature of aluminum but may not be quantitatively accurate above it. Specifically, we will use a simplified and computationally less demanding version of the theory and model our system as an SIS/IS structure with rigid boundary conditions, thin middle layer, and identical barriers on both sides. As shown by data fitting in Fig. 5, this oversimplified model allows us to justify saying that a high-transparency interface ($\tau \sim 0.98$) for the built junctions has been achieved. The suppression of the superconductivity in NbN due to the

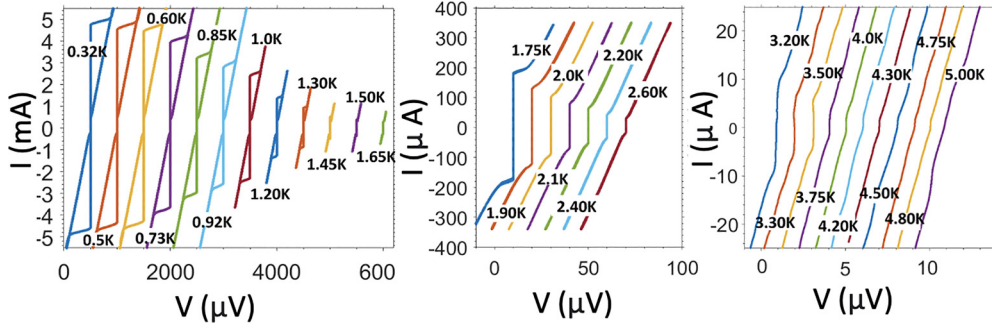


FIG. 4. Current-voltage curves for the NbN/Al-E2 junction display hysteretic behavior up to 3.3 K. The curves are shifted for clarity.

inverse proximity effect [1] in the leads is taken into account via an additional prefactor in the final expression for the Josephson current (see Appendix B). In this model the Josephson current is the sum of two contributions [50], $I_b(\phi/2)$ and $I_{pr}(\phi)$, which represent the current flowing through the two connected in series Josephson junctions (SIS' and S'IS) and a proximity-mediated current through the whole SIS'IS structure, respectively,

$$I_J(\phi) = I_b(\phi/2) + I_{pr}(\phi). \quad (1)$$

Further details about the developed model are reported in Appendix B. Here we briefly discuss the physical properties that it describes. At temperatures below T_C^{Al} the term $I_b(\phi/2)$ dominates in Eq. (1). It is given by the usual expression for a Josephson tunnel junction with leads that have different superconducting gaps Δ_{NbN} and Δ_{Al} and with the phase difference $\phi/2$ across the junction. The temperature dependence of the critical current in this regime depends on the average

transparency of the barrier τ_B . By fitting the experimental data, we find that values of τ_B close to 1 better describe the observations (see Fig. 5). This indicates the high transparency of the Au/Ti barriers between NbN and Al. The superconducting gap in the aluminum bridge is influenced by the proximity effect, and it should be found self-consistently. For this reason, Δ_{Al} remains finite even at temperatures $T > T_C^{\text{Al}}$ (see the inset of Fig. 5). At even higher temperatures Δ_{Al} becomes small, and the second term in Eq. (1), $I_{pr}(\phi)$, becomes dominant. This term represents the current through an SINIS structure. In the short junction limit it is determined by the escape rate of an electron from the normal middle layer, which we denote as Γ . In the short junction limit it is expressed via the Thouless energy of the aluminum layer and the channel and barrier resistances as $\Gamma \sim 4R_C E_{\text{Th}} / (2R_B + R_C)$. Based on the resistivity of the aluminum nanowire, we estimate its mean free path as $l_e = 13.3$ nm, the diffusion constant as $D = v_F l_e / 3 = 5.8 \times 10^{-3}$ m²/s, and the Thouless energy of the aluminum bridge of the junction as $E_{\text{Th}} = \hbar D / L^2 \sim 380$ μeV , with a geometrical gap length $L = 100$ nm. Using the parameters reported in Table I and the above value of the Thouless energy, we obtain $\Gamma = 357$ μeV . This value is much higher than that obtained from the fit procedure carried out in Fig. 6 and used to extract E_{Th} , where $\Gamma = 2.86$ μeV . However, the effective length of the junction is much longer due to the overlapping geometry of the NbN electrodes and the aluminum layer. This leads to an injection of currents into the Al over distances much longer than the nominal nanogap. Indeed, if we use an effective length of $L_{\text{eff}} = 800$ nm, we obtain $\Gamma = 5$ μeV , which is not far from the fitted value.

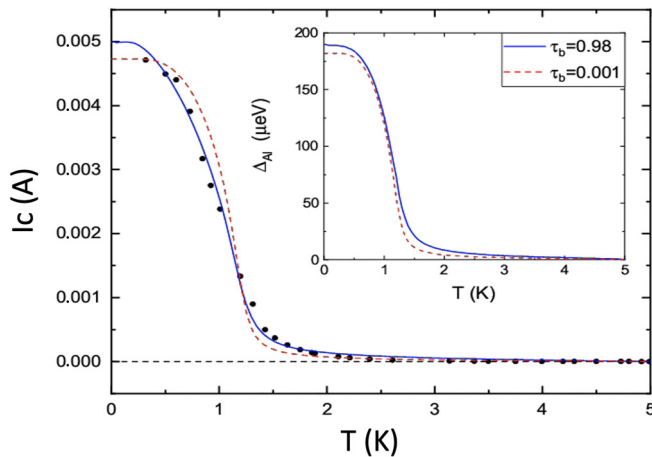


FIG. 5. Fit of the experimental I_C - T dependence for the junction NbN/Al-E2 (see Table I) with Eqs. (1)–(3). Black circles represent experimental data, the solid blue line shows Eqs. (1)–(3) with $\tau_b = 0.98$, and the dashed red line shows Eqs. (1)–(3) with $\tau_b = 0.001$. The system parameters are $T_C^{\text{NbN}} = 5$ K and $R_N = 0.081$ Ω . The fit parameters for transparent interfaces with $\tau_b = 0.98$ are $T_C^{\text{Al}} = 1.3$ K, $\Gamma = 2.86$ μeV , and $A = 0.22$. For the model with strong tunnel barriers, $\tau_b = 0.001$, we find the best fit with $T_C^{\text{Al}} = 1.2$ K, $\Gamma = 1.4$ μeV , and $A = 0.372$. The inset shows the temperature dependence of the superconducting order parameter in aluminum that follows from the self-consistency equation (B5).

3. Magnetotransport properties

Figures 7(a) and 7(b) show the differential resistance vs magnetic field dependence at two different temperatures for the NbN/Al-E2 junction. The curves are well described in the framework of the electrodynamics of the junctions [15]. Since the thickness of NbN t^{NbN} is smaller than $\lambda_L^{\text{NbN}} \sim 390$ nm (London penetration depth), the characteristic length that rules the variation of the phase difference ϕ along the junction is $l_J = \lambda_J^2 / \lambda_L$ [1,58,59], where $\lambda_J \sim 1 / \sqrt{1 - T/T_C}$ is the Josephson penetration depth. At $T^* = 1.7$ K we find $l_J = W$ [W represents the width of the junction, as shown in Fig. 1(b)], which signals the border between the magnetically long and short junction regimes [1,66,67]. For $T > T^*$ the I - B graph shows a Fraunhofer-like dependence with magnetic

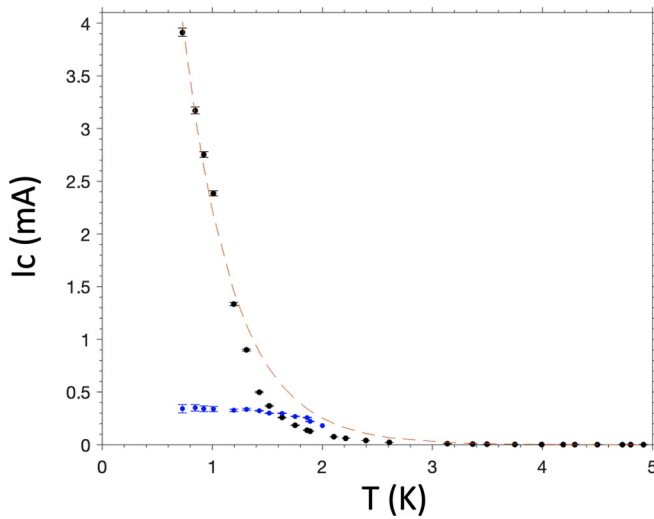


FIG. 6. The retrapping currents I_r (blue circles) and high-temperature switching currents I_s (black circles) as a function of temperature for the NbN/Al-E2 junction are shown. The red line represents the fit based on the relation reported in [65] used to estimate Thouless energy E_{Th} .

periodicity $\Delta B \sim 1.7$ mT [see Fig. 7(a)]. This value is in reasonable agreement with that predicted in the case of thin films where flux-focusing effects are relevant, $\Delta B \sim 1.84 \times \Phi_0 W^2$ [1,66–68], with Φ_0 and W being the magnetic flux quantum and the width of the junction, respectively. The attenuation of the high-order maxima can be ascribed to a possible nonuniform spatial distribution of the critical current amplitude inside the junction [69,70]. At low temperature we have $l_J \ll W$; then the I - B characteristic does not follow a Fraunhofer dependence [see Fig. 7(b)]. In this limit the Josephson currents can also generate a self-magnetic field that modifies the position of maxima of I_C .

IV. CONCLUSION

We have realized NbN nanogap-based Josephson junctions using a superconductor as a material barrier which displayed a Josephson current density higher than that of Al nanowires. Because of the high compatibility of the Au that covers the NbN banks, with a wide class of materials, such as topolog-

ical insulators [29,71,72], semiconducting nanowires [9,15–18,47,48], graphene [40,73,74], and ferromagnetic materials [10–13], and considering the high stability in the magnetic field of NbN ($H_{C2}^{NbN} \sim 25T$), our nanogap technology could represent an important suitable platform for exploring the novel properties of hybrid superconducting systems. In particular nanogaps could become the key element for investigating reliable hybrid junctions when the barrier is made of a suspended two-dimensional material [74]. NbN nanogaps would also give great freedom to design advanced circuits and, due to their high stability in magnetic field, might represent a key element for engineering complex circuits for quantum computing applications [75–78]. Moreover, the developed nanofabrication procedure is fully compatible with HTS technology; thus, it could also pave the way towards hybrid superconducting systems employing HTS [47,79].

ACKNOWLEDGMENTS

This work was partially supported by the Foundation BLANCEFLOR Boncompagni Ludovisi and by Progetto PON RI 2014-2020 “AIM: Attraction and International Mobility.”

The authors declare that they have no conflict of interest.

APPENDIX A: I - B FOR LOW-TRANSPARENCY STRUCTURES

In Fig. 8(a) the current-applied magnetic field (I - B) dependence of a NbN/Au-B2 superconducting quantum interference device (SQUID) is shown. We observe SQUID oscillations with a period $\Delta B \sim 280$ μ T, consistent with that computed via the geometrical area $A_{geo} = d \times L$ [d and L are defined in Fig. 8(c)]. We attribute the full agreement between A_{geo} and $A_{eff} = \frac{\Phi_0}{\Delta B}$ to the high ratio between d and W_{NbN} ($d \sim 39.6$ μ m represents the distance between two Au weak links, and $W_{NbN} \sim 2$ μ m is the width of NbN leads). Numerical simulations confirm that with such a SQUID layout for $d/W_{NbN} \gg 1$ the screening currents in the SC leads generate a small magnetic field that does not significantly affect the SQUID periodicity ΔB . Figure 8(a) shows that SQUID oscillations are enclosed in an envelope due to the Josephson current interferences of the individual junctions, whose width is half of that of the NbN/Al-B2 junction (see

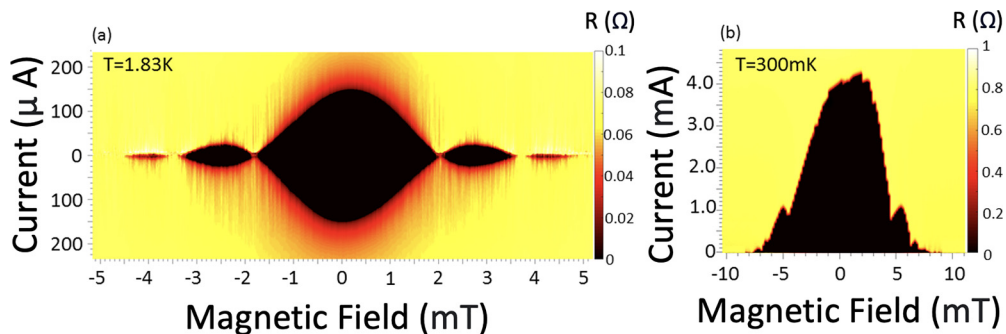


FIG. 7. Resistance maps as a function of bias current and applied magnetic (I - B) field for the junction NbN/Al-E2. (a) At $T = 1.83$ K the junction works in a short transport regime ($\lambda_J > W$) and the Fraunhofer-like dependence is shown. (b) At $T = 300$ mK the junction evolves in the long limit ($\lambda_J < W$), and the I - B dependence is no longer sinusoidal.

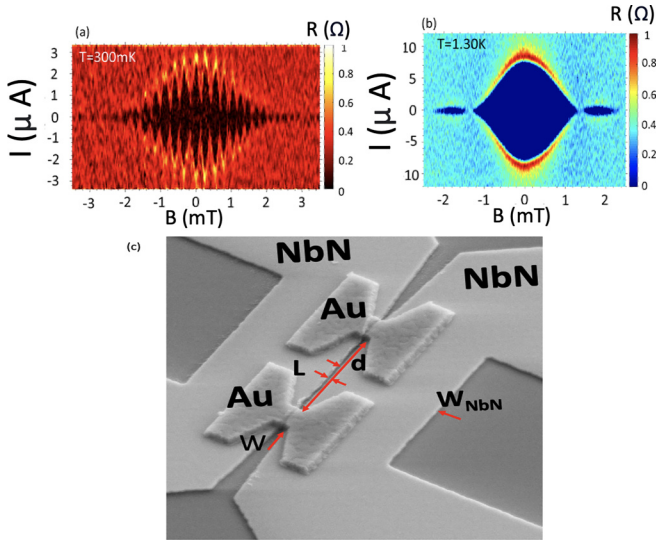


FIG. 8. Resistance maps as a function of bias current and applied magnetic (I - B) field for devices based on NbN nanogap: (a) NbN/Au-B2 SQUID and (b) NbN/Al-B2 junction. (c) Scanning electron microscope image showing the SQUID layout of a device similar to the one whose properties are reported in (a) and (b). The NbN/Au-B2 SQUID has $d = 39.6 \mu\text{m}$, $L = 230 \text{ nm}$, $W = 500 \text{ nm}$, and $W_{\text{NbN}} \sim 2 \mu\text{m}$.

Table I), confirming a wider periodicity in the I - B graph [1,80,81]. For such a SQUID we estimate $\beta_L = I_{\text{max}}/\Delta I_C = 2$ (where I_{max} and I_{min} are the maximum and minimum values of I_C and $\Delta I_C = I_{\text{max}} - I_{\text{min}}$) and the transfer function $V_{\Phi_0} = 700 \text{ nV}/\Phi_0$ [1].

Figure 8(b) shows the I - B dependence of the NbN/Al-B2 junction. I - B is recorded at $T = 1.3 \text{ K}$, and despite lower transparency of the junction, the modulation I - B is still in

$$I_b\left(\frac{\varphi}{2}\right) = \frac{8\pi A k_B T}{e R_N} \sum_{\omega_n} \frac{F_{\text{NbN}}(\omega_n) F_{\text{Al}}(\omega_n, \varphi) \sin \frac{\varphi}{2}}{2 - \tau_b + \tau_b \left(\frac{\hbar^2 \omega_n^2}{\Delta_{\text{NbN}} \Delta_{\text{Al}}} + \cos \frac{\varphi}{2} \right) F_{\text{NbN}}(\omega_n) F_{\text{Al}}(\omega_n, \varphi)} \quad (\text{B1})$$

and depends on the phase difference across one of the junctions, which in the symmetric setup equals $\phi/2$. For the second contribution to the current, $I_b(\phi)$, we use the expression derived for an SIS/IS structure with low-transparency tunnel interfaces [50],

$$I_{\text{pr}}(\varphi) = \frac{2\pi A k_B T}{e R_N} \sum_{\omega_n} \frac{\Gamma F_{\text{NbN}}^2(\omega_n) F_{\text{Al}}(\omega_n, \varphi)}{\Delta_{\text{Al}}} \sin \varphi. \quad (\text{B2})$$

The form of this contribution is not very important since in our system $I_{\text{pr}}(\phi) \ll I_b(\phi/2)$ at all temperatures except in the vicinity of the critical temperature of NbN, where the Josephson current is very small anyway. In Eqs. (B1) and (B2) we have used the following parameters: Matsubara frequencies $\omega_n = (2n+1)\pi k_B T/\hbar$, where n is an integer number; the average transmission probability of the barriers between the NbN and Al layers τ_b ; the normal state resistance of the whole structure R_N ; and the superconducting order parameters in NbN, Δ_{NbN} , and in Al, Δ_{Al} . In addition, we have introduced

agreement with that predicted by $\Delta B \sim 1.84\Phi_0 W$ [1,66,67] reported in Sec. III A 3.

APPENDIX B: THEORETICAL MODEL

A complete theory of the Josephson effect in our structure would rely on Usadel equations with proper boundary conditions at the interfaces between different materials. It would need to take into account the coordinate dependence of the quasiclassical Green's functions originating from the proximity effect. The full theory would require a numerical solution, which is quite difficult, especially in a sample with a complicated geometry like ours, and the result of such a simulation would be sensitive to the assumptions about the quality of the interfaces. For these reasons, here we use a simplified version of the theory, which is analytically tractable. We use the following approximations: (i) we treat the aluminum connection between the NbN leads as a thin superconducting layer with coordinate-independent Green's functions, (ii) we treat NbN leads as bulk superconductors with a coordinate-independent energy gap, and (iii) we treat the gold-titanium bilayers as thin barriers phenomenologically characterized by a single barrier transmission probability τ_b . Within this model, gap suppression in NbN leads in the vicinity of the barriers is described by a single suppression parameter, $A < 1$. Despite its simplicity, this model captures the main physical effects which determine the value of the critical current in our system. For example, it accounts for the proximity effect in the aluminum layer, which results in the final value of the superconducting gap even above its critical temperature. Adopting the approximations outlined above, we obtain the Josephson current through our structure in the form of Eq. (1). In this equation, the term that describes the Josephson current through a single NbN/Au/Ti/Al junction is given by the expression [82]

the parameter Γ , which characterizes the coupling strength between the Al and NbN layers. Physically, it can be interpreted as the escape rate of an electron from the Al layer into the NbN leads or, alternatively, as a value of the proximity-induced minigap in the middle Al layer if it is driven to the normal state. The prefactor A appearing in Eqs. (B1) and (B2) approximately accounts for the suppression of superconductivity in NbN leads by the inverse proximity effect and in the aluminum by high current density and the effects ignored in our simple model with rigid boundary conditions. For transparent barriers with $\tau_b = 1$ the prefactor A can be estimated as [5]

$$A \approx 0.8 \exp \left[-\frac{1}{1.45} \frac{\sigma_{\text{NbN}}}{\sigma_{\text{Al}}} \sqrt{\frac{D_{\text{Al}}}{D_{\text{NbN}}} \frac{T_C^{\text{NbN}}}{T_C^{\text{Al}}}} \right], \quad (\text{B3})$$

where $\sigma_{(\text{Al},\text{NbN})}$ are the conductivities of the Al and NbN layers, $D_{(\text{Al},\text{NbN})}$ are the corresponding diffusion constants, and $T_C^{(\text{Al},\text{NbN})}$ are the critical temperatures of the two materials.

Next, the Matsubara Green's functions in NbN and Al are defined as follows [5]:

$$F_{\text{NbN}}(\omega_n) = \frac{\Delta_{\text{NbN}}}{\sqrt{\hbar^2 \omega_n^2 + \Delta_{\text{NbN}}^2}},$$

$$F_{\text{Al}}(\omega_n, \varphi) = \frac{\Delta_{\text{Al}}}{\sqrt{\hbar^2 \omega_n^2 \left(1 + \frac{\Gamma F_{\text{NbN}}(\omega_n)}{\Delta_{\text{NbN}}}\right)^2 + (\Delta_{\text{Al}} + \Gamma F_{\text{NbN}}(\omega_n) \cos \frac{\varphi}{2})^2}}. \quad (\text{B4})$$

In our model, the Green's function of the NbN leads $F_{\text{NbN}}(\omega_n)$ is the same as in a bulk superconductor, while the Green's function of the aluminum layer is modified by the proximity effect and therefore depends on the Josephson phase ϕ . Finally, the superconducting order parameter of the aluminum layer Δ_{Al} should be found from the self-consistency equation,

$$\Delta_{\text{Al}} \ln \frac{T}{T_C^{\text{Al}}} + 2\pi k_B T \sum_{\omega_n > 0} \left[\frac{\Delta_{\text{Al}}}{\hbar \omega_n} - \frac{[\Delta_{\text{Al}} + \Gamma \cos \frac{\varphi}{2} F_{\text{NbN}}(\omega_n)] F_{\text{Al}}(\omega_n)}{\Delta_{\text{Al}}} \right] = 0. \quad (\text{B5})$$

In order to clarify the physical meaning of Eq. (1), we consider several limiting cases. At low temperatures, where both NbN and Al are in the superconducting state, the structure is essentially reduced to the two NbN/Au/Ti/Al Josephson junctions connected in series. The Josephson current is then given by $I_b(\phi/2)$, while the term $I_{pr}(\phi)$, which results from the Cooper pair tunneling events through the whole Au/Ti/Al/Ti/Au multilayer barrier, is small and can be neglected. With growing temperature Δ_{Al} decreases together with the value of the critical current. Since the aluminum layer is thin, Δ_{Al} does not vanish even above the critical temperature of this material. Indeed, the self-consistency equation (B5) always results in a nonzero value of the gap due to the finite value of the escape rate. For this reason, the contribution in Eq. (1) continues to dominate over $I_{pr}(\phi)$ in a large part of the temperature interval $T > T_C^{\text{Al}}$, completely vanishing only close to the critical temperature of NbN. This behavior differs from that of an SINIS junction. In the latter case, the superconducting order parameter in the middle layer always equals to zero even though the proximity effect induces the finite minigap in it. Hence, the first term in Eq. (1) vanishes, and the Josephson current is the given by the remaining contribution (B2). We fit the experimental temperature dependence of the critical current with the above expressions (see Fig. 5). We were able to fit the data quite well assuming transparent interfaces between the NbN leads and the Al

layer (see the blue line in Fig. 5). For comparison, we also plotted theory prediction for a system with low-transparency barriers (red dashed line in Fig. 5) and found that it fits the data much worse. The essential fitting parameters in the model are the values of the suppression prefactor A and of the proximity-induced minigap in aluminum Γ . Assuming transparent barriers, we find $A = 0.22$, in good agreement with the prediction of Eq. (B3), which for $\sigma_{\text{Al}} \sim \sigma_{\text{NbN}}$, $D_{\text{Al}} \sim D_{\text{NbN}}$, and $T_C^{\text{Al}} = 1.3$ K and $T_C^{\text{NbN}} = 5$ K gives $A = 0.196$. According to the theory, the parameter γ should be close to the Thouless energy of the aluminum layer, which we estimate to be $E_{\text{Th}} \sim 15$ μeV (see Sec. III), assuming the distance between the NbN leads is $L = 100$ nm. From the fits we obtain a value one order of magnitude lower, $\Gamma = 2.86$ μeV . A possible explanation for this discrepancy could again be the suppression of the superconductivity in NbN by the inverse proximity effect, which not only results in the suppression of I_C by the prefactor A but also makes the effective distance between the superconducting leads longer and in this way reduces E_{Th} . In the inset of Fig. 5 we plot the temperature dependence of the order parameter in the aluminum layer obtained with the numerical solution of the self-consistency equation (B5). The strong proximity effect from the NbN leads makes Δ_{Al} finite even above the critical temperature of Al and ensures a smooth transition from high to low values of the critical current around T_C^{Al} .

- [1] A. Barone and G. Paterno, *Physics and Applications of the Josephson Effects* (Wiley, New York, 1982).
- [2] V. Cherkez, J. C. Cuevas, C. Brun, T. Cren, G. Menard, F. Debontridder, V. S. Stolyarov, and D. Roditchev, Proximity Effect between Two Superconductors Spatially Resolved by Scanning Tunneling Spectroscopy, *Phys. Rev. X* **4**, 011033 (2014).
- [3] S. K. Tolpygo and V. K. Semenov, Increasing integration scale of superconductor electronics beyond one million Josephson junctions, *J. Phys.: Conf. Ser.* **1559**, 012002 (2020).
- [4] K. K. Likharev, Superconducting weak links, *Rev. Mod. Phys.* **51**, 101 (1979).

- [5] A. A. Golubov, M. Y. Kupriyanov, and E. Il'ichev, The current-phase relation in Josephson junctions, *Rev. Mod. Phys.* **76**, 411 (2004).
- [6] H. Takayanagi and T. Kawakami, Superconducting Proximity Effect in the Native Inversion Layer on InAs, *Phys. Rev. Lett.* **54**, 2449 (1985).
- [7] C. W. J. Beenakker, Universal Limit of Critical-Current Fluctuations in Mesoscopic Josephson Junctions, *Phys. Rev. Lett.* **67**, 3836 (1991).
- [8] J. A. Bert, B. Kalisky, C. Bell, M. Kim, Y. Hikita, H. Y. Hwang, and K. A. Moler, Direct imaging of the coexistence of ferromagnetism and superconductivity at the LaAlO₃/SrTiO₃ interface, *Nat. Phys.* **7**, 767 (2011).

- [9] W. Chang, S. M. Albrecht, T. S. Jespersen, F. Kuemmeth, P. Krogstrup, J. Nygard, and C. M. Marcus, Hard gap in epitaxial semiconductor-superconductor nanowires, *Nat. Nanotechnol.* **10**, 232 (2015).
- [10] R. Satariano, L. Parlato, A. Vettoliere, R. Caruso, H. G. Ahmad, A. Miano, L. Di Palma, D. Salvoni, D. Montemurro, C. Granata, G. Lamura, F. Tafuri, G. P. Pepe, D. Massarotti, and G. Ausanio, Inverse magnetic hysteresis of the Josephson supercurrent: Study of the magnetic properties of thin niobium/permalloy ($\text{Fe}_{20}\text{Ni}_{80}$) interfaces, *Phys. Rev. B* **103**, 224521 (2021).
- [11] L. Parlato, R. Caruso, A. Vettoliere, R. Satariano, H. G. Ahmad, A. Miano, D. Montemurro, D. Salvoni, G. Ausanio, F. Tafuri, G. P. Pepe, D. Massarotti, and C. Granata, Characterization of scalable Josephson memory element containing a strong ferromagnet, *J. Appl. Phys.* **127**, 193901 (2020).
- [12] T. Kontos, M. Aprili, J. Lesueur, F. Genet, B. Stephanidis, and R. Boursier, Josephson Junction through a Thin Ferromagnetic Layer: Negative Coupling, *Phys. Rev. Lett.* **89**, 137007 (2002).
- [13] V. V. Ryazanov, V. A. Oboznov, A. Y. Rusanov, A. V. Veretennikov, A. A. Golubov, and J. Aarts, Coupling of Two Superconductors through a Ferromagnet: Evidence for a π Junction, *Phys. Rev. Lett.* **86**, 2427 (2001).
- [14] A. Vettoliere, R. Satariano, R. Ferraiuolo, L. Di Palma, H. G. Ahmad, G. Ausanio, G. P. Pepe, F. Tafuri, D. Montemurro, C. Granata, L. Parlato, and D. Massarotti, Aluminum-ferromagnetic Josephson tunnel junctions for high quality magnetic switching devices, *Appl. Phys. Lett.* **120**, 262601 (2022).
- [15] Y.-J. Doh, J. A. van Dam, A. L. Roest, E. P. A. M. Bakkers, L. P. Kouwenhoven, and S. De Franceschi, Tunable supercurrent through semiconductor nanowires, *Science* **309**, 272 (2005).
- [16] V. Mourik, K. Zuo, S. M. Frolov, S. R. Plissard, E. P. A. M. Bakkers, and L. P. Kouwenhoven, Signatures of majorana fermions in hybrid superconductor-semiconductor nanowire devices, *Science* **336**, 1003 (2012).
- [17] P. Krogstrup, N. L. B. Ziino, W. Chang, S. M. Albrecht, M. H. Madsen, E. Johnson, J. Nygard, C. Marcus, and T. S. Jespersen, Epitaxy of semiconductor-superconductor nanowires, *Nat. Mater.* **14**, 400 (2015).
- [18] A. F. Morpurgo, J. Kong, C. M. Marcus, and H. Dai, Gate-controlled superconducting proximity effect in carbon nanotubes, *Science* **286**, 263 (1999).
- [19] S. Abay, H. Nilsson, F. Wu, H. Xu, C. Wilson, and P. Delsing, High critical-current superconductor-InAs nanowire-superconductor junctions, *Nano Lett.* **12**, 5622 (2012).
- [20] J. A. van Dam, Y. V. Nazarov, E. P. A. M. Bakkers, S. De Franceschi, and L. P. Kouwenhoven, Supercurrent reversal in quantum dots, *Nature (London)* **442**, 667 (2006).
- [21] L. Fu and C. L. Kane, Superconducting Proximity Effect and Majorana Fermions at the Surface of a Topological Insulator, *Phys. Rev. Lett.* **100**, 096407 (2008).
- [22] H. Y. Günel, I. E. Batov, H. Hardtdegen, K. Sladek, A. Winden, K. Weis, G. Panaitov, D. Grutzmacher, and T. Schapers, Supercurrent in Nb/InAs-nanowire/Nb Josephson junctions, *J. Appl. Phys.* **112**, 034316 (2012).
- [23] R. M. Lutchyn, J. D. Sau, and S. Das Sarma, Majorana Fermions and a Topological Phase Transition in Semiconductor-Superconductor Heterostructures, *Phys. Rev. Lett.* **105**, 077001 (2010).
- [24] J. Alicea, Y. Oreg, G. Refael, F. von Oppen, and M. P. A. Fisher, Non-Abelian statistics and topological quantum information processing in 1D wire networks, *Nature (London)* **7**, 412 (2011).
- [25] A. Y. Kitaev, Unpaired Majorana fermions in quantum wires, *Phys. Usp.* **44**, 131 (2001).
- [26] J. Klinovaja and D. Loss, Parafermions in an Interacting Nanowire Bundle, *Phys. Rev. Lett.* **112**, 246403 (2014).
- [27] G. Kunakova, A. P. Surendran, D. Montemurro, M. Salvato, D. Golubev, J. Andzane, D. Erts, T. Bauch, and F. Lombardi, Topological insulator nanoribbon Josephson junctions: Evidence for size effects in transport properties, *J. Appl. Phys.* **128**, 194304 (2020).
- [28] S. Charpentier, L. Galletti, G. Kunakova, R. Arpaia, Y. Song, R. Baghdadi, S. M. Wang, A. Kalaboukhov, E. Olsson, F. Tafuri, D. Golubev, J. Linder, T. Bauch, and F. Lombardi, Induces unconventional superconductivity on the surface states of Bi_2Te_3 Topological insulator, *Nat. Commun.* **8**, 2019 (2017).
- [29] L. Galletti, S. Charpentier, M. Iavarone, P. Lucignano, D. Massarotti, R. Arpaia, Y. Suzuki, K. Kadowaki, T. Bauch, A. Tagliacozzo, F. Tafuri, and F. Lombardi, Influence of topological edge states on the properties of Al/ Bi_2Se_3 /Al hybrid Josephson devices, *Phys. Rev. B* **89**, 134512 (2014).
- [30] G. Kunakova, L. Galletti, S. Charpentier, J. Andzane, D. Erts, F. Léonard, C. D. Spataru, T. Bauch and F. Lombardi, Bulk-free topological insulator Bi_2Se_3 nanoribbons with magnetotransport signatures of Dirac surface states, *Nanoscale* **10**, 19595 (2018).
- [31] D. Hsieh, Y. Xia, L. Wray, D. Qian, A. Pal, J. H. Dil, J. Osterwalder, F. Meier, G. Bihlmayer, C. L. Kane, Y. S. Hor, R. J. Cava, and M. Z. Hasan, Observation of unconventional quantum spin textures in topological insulators, *Science* **323**, 919 (2009).
- [32] P. Rickhaus, M. H. Liu, P. Makk, R. Maurand, S. Hess, S. Zihlmann, M. Weiss, K. Richter and C. Schonenberger, Gate tuneable beamsplitter in ballistic graphene, *Appl. Phys. Lett.* **107**, 251901 (2015).
- [33] A. K. Geim, Graphene: Status and prospects, *Science* **324**, 1530 (2009).
- [34] J. Chen, M. A. Hamon, H. Hu, Y. Chen, A. M. Rao, P. C. Eklund, and R. C. Haddon, Solution properties of single-walled carbon nanotubes, *Science* **282**, 95 (1998).
- [35] V. N. Popov, Carbon nanotubes: Properties and application, *Mater. Sci. Eng., R* **43**, 61 (2004).
- [36] F. Tafuri and J. R. Kirtley, Weak links in high critical temperature superconductors, *Rep. Prog. Phys.* **68**, 2573 (2005).
- [37] T. W. Larsen, K. D. Petersson, F. Kuemmeth, T. S. Jespersen, P. Krogstrup, J. Nygard, and C. M. Marcus, Semiconductor-Nanowire-Based Superconducting Qubit, *Phys. Rev. Lett.* **115**, 127001 (2015).
- [38] O. Gül, H. Zhang, F. K. de Vries, J. van Veen, K. Zuo, V. Mourik, S. Conesa-Boj, M. P. Nowak, D. J. van Woerkom, M. Quintero-Perez, M. C. Cassidy, A. Geresdi, S. Koelling, D. Car, S. R. Plissard, E. P. A. M. Bakkers, and L. P. Kouwenhoven, Hard superconducting gap in InSb nanowires, *Nano Lett.* **17**, 2690 (2017).

- [39] G. Kunakova, T. Bauch, E. Tralbaldo, J. Andzane, D. Erts, and F. Lombardi, High transparency Bi_2Se_3 topological insulator nanoribbon Josephson junctions with low resistive noise properties, *Appl. Phys. Lett.* **115**, 172601 (2019).
- [40] H. B. Heersche, P. J. Herrero, J. B. Oostinga, L. M. K. Vandersypen, and A. F. Morpurgo, Bipolar supercurrent in graphene, *Nature (London)* **446**, 56 (2007).
- [41] S. K. Tolpygo, D. Yohannes, R. T. Hunt, J. A. Vivalda, D. Donnelly, D. Amparo, A. F. Kirichenko, 20 kA/cm² process development for superconducting integrated circuits with 80 GHz clock frequency, *IEEE Trans. Appl. Supercond.* **17**, 946 (2007).
- [42] J. N. Hancock, J. L. M. van Mechelen, A. B. Kuzmenko, D. van der Marel, C. Brune, E. G. Novik, G. V. Astakhov, H. Buhmann, and L. W. Molenkamp, Surface State Charge Dynamics of a High-Mobility Three-Dimensional Topological Insulator, *Phys. Rev. Lett.* **107**, 136803 (2011).
- [43] E. Tralbaldo, S. Ruffieux, E. Andersson, R. Arpaia, D. Montemurro, J. F. Schneiderman, A. Kalaboukhov, D. Winkler, F. Lombardi, and T. Bauch, Properties of grooved Dayem bridge based $\text{YBa}_2\text{Cu}_3\text{O}_{7-\delta}$ superconducting quantum interference devices and magnetometers, *Appl. Phys. Lett.* **116**, 132601 (2020).
- [44] F. Arcadio, L. Zeni, D. Montemurro, C. Eramo, S. Di Ronza, C. Perri, G. D'Agostino, G. Chiaretti, G. Porto, and N. Cennamo, Biochemical sensing exploiting plasmonic sensors based on gold nanogratings and polymer optical fibers, *Photonics Res.* **9**, 1397 (2021).
- [45] R. Baghdadi, R. Arpaia, S. Charpentier, D. Golubev, T. Bauch, and F. Lombardi, Fabricating Nanogaps in $\text{YBa}_2\text{Cu}_3\text{O}_{7-\delta}$ for Hybrid Proximity-Based Josephson Junctions, *Phys. Rev. Appl.* **4**, 014022 (2015).
- [46] E. Bhatia, A. Srivastava, J. D. Stoneman, N. A. Stelmashenko, Z. H. Barber, J. W. A. Robinson, and K. Senapati, Nanoscale domain wall engineered spin-triplet Josephson junctions and SQUID, *Nano Lett.* **21**, 3092 (2021).
- [47] D. Montemurro, D. Massarotti, P. Lucignano, S. Roddaro, D. Stornaiuolo, D. Ercolani, L. Sorba, A. Tagliacozzo, F. Beltram, and F. Tafuri, Towards a hybrid high critical temperature superconductor junction with a semiconducting InAs nanowire barrier, *J. Supercond. Novel Magn.* **28**, 3429 (2015).
- [48] D. Montemurro, D. Stornaiuolo, D. Massarotti, D. Ercolani, L. Sorba, F. Beltram, F. Tafuri, and S. Roddaro, Suspended InAs nanowire Josephson junctions assembled via dielectrophoresis, *Nanotechnology* **26**, 385302 (2015).
- [49] P. G. De Gennes, Boundary effects in superconductors, *Rev. Mod. Phys.* **36**, 225 (1964).
- [50] M. Yu. Kupriyanov, A. Brinkman, A. A. Golubov, M. Siegel, and H. Rogalla, Double-barrier Josephson structures as the novel elements for superconducting large-scale integrated circuits, *Phys. C (Amsterdam, Neth.)* **326-327**, 16 (1999).
- [51] A. Andreev, The thermal conductivity of the intermediate state in superconductors, *J. Exp. Theor. Phys.* **19**, 1228 (1964).
- [52] P. Li, P. M. Wu, Y. Bomze, I. V. Borzenets, G. Finkelstein, and A. M. Chang, Switching Currents Limited by Single Phase Slips in One-Dimensional Superconducting Al Nanowires, *Phys. Rev. Lett.* **107**, 137004 (2011).
- [53] T. M. Wall, B. Leith, N. Hartman, A. Rahman, and N. Markovic, Measurement of Critical Currents of Superconducting Aluminum Nanowires in External Magnetic Fields: Evidence for a Weber Blockade, *Phys. Rev. Lett.* **114**, 077002 (2015).
- [54] L. Grünhaupt, M. Spiecker, D. Gusenkova, N. Maleeva, S. T. Skacel, I. Takmakov, F. Valenti, P. Winkel, H. Rotzinger, W. Wernsdorfer, A. V. Ustinov, and I. M. Pop, Granular aluminium as a superconducting material for high-impedance quantum circuits, *Nat. Mater.* **18**, 816 (2019).
- [55] I. E. Batov, T. Schapers, A. A. Golubov, and A. V. Ustinov, Andreev reflection and enhanced subgap conductance in NbN/Au/InGaAs-InP junctions, *J. Appl. Phys.* **96**, 3366 (2004).
- [56] Y. Lobanov, M. Shcherbatenko, A. Shurakov, A. V. Rodin, A. Klimchuk, A. I. Nadezhdinsky, S. Maslennikov, P. Larionov, M. Finkel, A. Semenov, A. A. Verevkin, B. M. Voronov, Y. Ponurovsky, T. M. Klapwijk, and G. N. Gol'tsman, Heterodyne detection at near-infrared wavelengths with a superconducting NbN hot-electron bolometer mixer, *Opt. Lett.* **39**, 1429 (2014).
- [57] R. Arpaia, S. Nawaz, F. Lombardi, and T. Bauch, Improved nanopatterning for YBCO nanowires approaching the depairing current, *IEEE Trans. Appl. Supercond.* **23**, 1101505 (2013).
- [58] W. N. Ashcroft and D. Mermin, *Solid State Physics* (Harcourt College, 1976).
- [59] S. Nawaz, R. Arpaia, F. Lombardi, and T. Bauch, Microwave Response of Superconducting $\text{YBa}_2\text{Cu}_3\text{O}_{7-\delta}$ Nanowire Bridges Sustaining the Critical Depairing Current: Evidence of Josephson-like Behavior, *Phys. Rev. Lett.* **110**, 167004 (2013).
- [60] O. V. Skryabina, S. V. Bakurskiy, A. G. Shishkin, A. A. Klimenko, K. S. Napolskii, N. V. Klenov, I. I. Soloviev, V. V. Ryazanov, A. A. Golubov, D. Roditchev, M. Yu. Kupriyanov, and V. S. Stolyarov, Environment-induced overheating phenomena in Au-nanowire based Josephson junctions, *Sci. Rep.* **11**, 15274 (2021).
- [61] G. H. Lee, K. F. Huang, D. K. Efetov, D. S. Wei, S. Hart, T. Taniguchi, K. Watanabe, A. Yacoby, and P. Kim, Inducing superconducting correlation in quantum Hall edge states, *Nat. Phys.* **13**, 693 (2017).
- [62] Z. Wan, A. Kazakov, M. J. Manfra, L. N. Pfeiffer, K. W. West, and L. P. Rokhinson, Induced superconductivity in high-mobility two-dimensional electron gas in gallium arsenide heterostructures, *Nat. Commun.* **6**, 7426 (2015).
- [63] H. Courtois, M. Meschke, J. T. Peltonen, and J. P. Pekola, Origin of Hysteresis in a Proximity Josephson Junction, *Phys. Rev. Lett.* **101**, 067002 (2008).
- [64] K. D. Usadel, Generalized Diffusion Equation for Superconducting Alloys, *Phys. Rev. Lett.* **25**, 507 (1970).
- [65] P. Dubos, H. Courtois, B. Pannetier, F. K. Wilhelm, A. D. Zaikin, and G. Schon, Josephson critical current in a long mesoscopic S-N-S junction, *Phys. Rev. B* **63**, 064502 (2001).
- [66] R. C. Dynes and T. A. Fulton, Supercurrent density distribution in Josephson junctions, *Phys. Rev. B* **3**, 3015 (1971).
- [67] V. G. Kogan, V. V. Dobrovitski, J. R. Clem, Y. Mawatari, and R. G. Mints, Josephson junction in a thin film, *Phys. Rev. B* **63**, 144501 (2001).
- [68] A. Barone, G. Paterno, M. Russo, and R. Vaglio, Diffraction and interference phenomena in single Josephson junctions, *Phys. Status Solidi A* **41**, 393 (1977).
- [69] A. Barone, W. J. Johnson, and R. Vaglio, Current flow in large Josephson junctions, *J. Appl. Phys.* **46**, 3628 (1975).
- [70] C. S. Owen and D. J. Scalapino, Vortex structure and critical currents in Josephson junctions, *Phys. Rev.* **164**, 538 (1967).
- [71] M. Z. Hasan and C. L. Kane, Colloquium: Topological insulators, *Rev. Mod. Phys.* **82**, 3045 (2010).

- [72] L. A. Wray, S.-Y. Xu, Y. Xia, Y. S. Hor, D. Qian, A. V. Fedorov, H. Lin, A. Bansil, R. J. Cava, and M. Z. Hasan, Observation of topological order in a superconducting doped topological insulator, *Nat. Phys.* **6**, 855 (2010).
- [73] B. Uchoa and A. H. Castro Neto, Superconducting States of Pure and Doped Graphene, *Phys. Rev. Lett.* **98**, 146801 (2007).
- [74] X. Du, I. Skachko, and E. Y. Andrei, Josephson current and multiple Andreev reflections in graphene SNS junctions, *Phys. Rev. B* **77**, 184507 (2008).
- [75] L. Casparis, T. W. Larsen, M. S. Olsen, F. Kuemmeth, P. Krogstrup, J. Nygård, K. D. Petersson, and C. M. Marcus, Gate-mon Benchmarking and Two-Qubit Operations, *Phys. Rev. Lett.* **116**, 150505 (2016).
- [76] G. de Lange, B. van Heck, A. Bruno, D. J. van Woerkom, A. Geresdi, S. R. Plissard, E. P. A. M. Bakkers, A. R. Akhmerov, and L. DiCarlo, Realization of Microwave Quantum Circuits Using Hybrid Superconducting-Semiconducting Nanowire Josephson Elements, *Phys. Rev. Lett.* **115**, 127002 (2015).
- [77] J. Tejada, E. M. Chudnovsky, E. del Barco, J. M. Hernandez, and T. P. Spiller, Magnetic qubits as hardware for quantum computers, *Nanotechnology* **12**, 181 (2001).
- [78] H. G. Ahmad, V. Brosco, A. Miano, L. Di Palma, M. Arzeo, D. Montemurro, P. Lucignano, G. P. Pepe, F. Tafuri, R. Fazio, and D. Massarotti, A hybrid ferromagnetic transmon qubit: Circuit design, feasibility and detection protocols for magnetic fluctuations, *Phys. Rev. B* **105**, 214522 (2022).
- [79] D. Perconte, F. A. Cuellar, C. Moreau-Luchaire, M. Piquemal-Banci, R. Galceran, P. R. Kidambi, M.-B. Martin, S. Hofmann, R. Bernard, B. Dlubak, P. Seneor, and J. E. Villegas, Tunable Klein-like tunnelling of high-temperature superconducting pairs into graphene, *Nat. Phys.* **14**, 25 (2018).
- [80] C. Kurter, A. Finck, Y. S. Hor, and D. J. Van Harlingen, Evidence for an anomalous current-phase relation in topological insulator Josephson junctions, *Nat. Commun.* **6**, 7130 (2015).
- [81] K. Nam-Hee, K. Hong-Seok, Y. Yiming, P. Xingyue, Y. Dong, and D. Yong-Joo, Fabrication and characterization of superconducting quantum interference device using $(\text{Bi}_{1-x}\text{Sb}_x)_2\text{Se}_3$ topological insulator nanoribbons, [arXiv:1801.07855](https://arxiv.org/abs/1801.07855).
- [82] A. V. Zaitsev, Quasiclassical equations of the theory of superconductivity for contiguous metals and the properties of constricted microcontacts, *Zh. Eksp. Teor. Fiz.* **59**, 1015 (1984).